Tribology International, March 2013, Vol. 59, pp. 248–258, DOI: 10.1016/j.triboint.2012.09.002
(Accepted Version)

Tribology of piston compression ring conjunction under transient thermal mixed regime of lubrication

N. Morris[1], R. Rahmani[1], H. Rahnejat[1§], P.D. King[1] and B. Fitzsimons[2]

[1] Wolfson School of Mechanical & Manufacturing Engineering, Loughborough University, Loughborough, UK

[2] Aston Martin Lagonda, Gaydon, Warwickshire, UK

[§]Corresponding author: H.Rahnejat@lboro.ac.uk, Tel: +44 (1509) 227569

Abstract

Fuel efficiency is the main IC engine attribute, with the compression ring-bore contact consuming nearly 5% of the fuel energy. Analyses are often idealised, such as isothermal condition and smooth surfaces, the former being particularly contrary to practice. An analytic solution to the average flow model is presented for this contact with a new analytical thermal model. The generated contact temperatures, particularly at the inlet result in thinner films than the idealised analyses. For the simulated city driving condition the power loss is mainly due to viscous shear under cold engine condition, whilst for a hot engine boundary friction dominates.

Keywords: Piston ring; Mixed lubrication; Friction; Heat

Nomenclature

A : Apparent contact area

A_a : Asperity contact area

A_h : Hydrodynamic contact area

b : Ring face-width

B : Damping coefficient

c_p : Lubricant specific heat at constant pressure

c_{s1} : Specific heat for the bore/liner material

c_{s2} : Specific heat for the ring's material

d : Ring radial width (thickness)

E' : Reduced (effective) elastic modulus of the contacting pair

f : Total friction

f_e : Ring elastic force

f_g : Gas force acting behind the ring

f_b : Boundary friction

f_v : Viscous friction

g : Incomplete circular ring's free end gap (pre-fitment)

h : Film thickness

h_0 : Minimum film thickness

h_t : Heat transfer coefficient of boundary layer

h_T : Rough surface film thickness

k_l : Thermal conductivity of the lubricant

k_{s1} : Thermal conductivity of the bore/liner

k_{s2} : Thermal conductivity of the ring

l : Ring length or bore perimeter

ℓ : Connecting rod length

L_{ev} : Entrance length for a fully developed velocity profile

L_{eth} : Entrance length for a fully developed temperature profile

$\dot{m}$: Lubricant mass flow rate

n : Iteration number

Nu : Nusselt number

p : Pressure

$\overline{p}$: Average pressure

p_c : Cavitation vaporisation pressure

p_e : Ring elastic pressure due to fitment

p_g : Gas pressure acting behind the ring

p_{in} : Inlet pressure

p_{out} : Outlet pressure

Pe : Peclet number

$\dot{Q}$: Heat flow rate

$\dot{Q}_1$: Conductive heat flow rate through the liner

$\dot{Q}_2$: Conductive heat flow rate through the ring

$\dot{Q}_{cv}$: Convective heat flow rate

r : Crank-pin radius

r_0 : Nominal bore radius

R' : Ring radius

R_e : Convective thermal resistance for the lubricant flow through the conjunction

R_l : Conductive thermal resistance for the lubricant layer

R_v : Convective thermal resistance of the boundary layer (between film and surface)

Re : Reynolds number

s : Profile of the ring face-width

t : Time

U : Speed of entraining motion

V : Variance ratios of rough surfaces

W_a : Load share of asperities

x : Direction along the ring face-width (direction of entraining motion)

x_c : Film rupture boundary

Greek symbols

α_0 : Pressure viscosity coefficient of lubricant

β : Thermal expansion coefficient of lubricant

χ : Transferred heat portion

δ_1, δ_2 : Roughness amplitude on the bore and ring surfaces

ΔU : Sliding velocity

$\Delta\theta$: Temperature rise

$\Delta\theta_{f1}, \Delta\theta_{f2}$: Flash temperature rise of the contacting surfaces

ε : Limit of convergence

φ_c : Contact factor

$\varphi_f, \varphi_{fs}, \varphi_{fp}$: Friction flow factors

φ_s : Shear flow factor

φ_x : Pressure flow factor

γ : Surface roughness orientation parameter

η_0 : Lubricant dynamic viscosity at atmospheric pressure and ambient temperature

η_e : Lubricant effective dynamic viscosity at temperature θ_e and pressure p

κ : Average asperity tip radius

λ : Stribeck oil film parameter

ν : Lubricant kinematic viscosity

θ_0 : Inlet lubricant temperature

θ_e : Effective lubricant contact temperature

θ_{s1}, θ_{s2} : Initial surface temperatures of the bore/liner and ring

ϑ : Load balance parameter

ρ : Lubricant density

ρ_{s1}, ρ_{s2} : Bore/liner and ring density

σ_1, σ_2 : Roughness Ra or Rk of liner and ring

σ : Root mean square roughness of contiguous surfaces

ς : Boundary shear strength of surfaces

$\overline{\tau}$: Average shear stress

τ_0 : Eyring shear stress of the lubricant

ω : Engine speed

ζ : Asperity density per unit contact area

ψ : Crank angle

Abbreviations

BDC : Bottom Dead Centre

BHP : Brake Horse Power

IC : Internal Combustion

TEHD : Thermo-Elastohydrodynamic

TDC : Top Dead Centre

1- Introduction

The parasitic losses of piston compression ring-bore contact accounts for nearly 5% of input fuel energy [1]. For such a small, but crucial component, this level of parasitic losses is rather alarming. With ever increasing cost and scarcity of fossil fuels much attention is directed to reducing these parasitic losses. A fundamental understanding of the transient nature of ring-bore contact is regarded as a prelude to its refinement. This conjunction is amongst the most complex problems on the account of the transient nature of contact kinematics, variable ring-bore conformance [2,3] and ring modal behaviour [4,5], all of which yield fairly thin films, often subject to mixed regime of lubrication [6-9].

There have been many studies of the compression ring-bore conjunction with increasing levels of practical detail and emphasis put on specific aspects, as noted above. They include transient hydrodynamic/elastohydrodynamic analysis by Dowson *et al* [10] for an assumed fully conformed ring-bore conjunction. This condition is ideal and does not usually occur. Hence, it was later extended to include ring-bore conformability analysis as well as including a more representative mixed regime of lubrication by Ma *et al* [6]. Further studies include solutions using the average flow model, proposed by Patir and Cheng [11] to include the effect of distributed roughness on lubricant flow and friction [12]. This approach leads to

more accurate evaluation of friction in rough wet surfaces. Another important issue is the inclusion of lubricant starvation prior to reversal due to a reduced rate of lubricant entrainment as well as lubricant cavitation, during the ring reversal [13].

Some studies have included the effect of ring-bore conformability to account for bore out-of-roundness, as well as asperity interactions for thin films during ring reversal [8,14]. Inclusion of these practical features has led to predictions of isothermal transient analyses which have been compared with experimental motored rigs of Furuhama and Sasaki [15] with good agreement [7,9]. However, under the usual fired engine condition the generated heat affects the lubricant viscosity and significantly alters the conditions observed using laboratory motored engines. Ghosh and Gupta [16] observed significant differences in load-carrying capacity, film thickness and rolling traction at high sliding speeds, when taking into account heat generated in the contact. For a thermal-elastohydrodynamic (TEHD) analysis, combined solution of Reynolds and energy equations is usually required. Such an approach has been reported by Almqvist and Larsson [17]. For good ring-bore conformance, Mishra *et al* [9], Chong *et al* [13] and Spencer *et al* [18] show that there is negligible *localised* ring deformation and there is no significant piezo-viscous action of the lubricant. Therefore, the prevailing conditions are either hydrodynamic or mixed regime of lubrication. This provides the opportunity to undertake one dimensional analytical solution of Reynolds equation, based on the Patir and Cheng [11] average flow model through rough surfaces [12].

The current analysis uses such an approach, also including the effect of asperity friction, based on the approach of Greenwood and Tripp [19]. Additionally, the current analysis includes a novel analytical thermal balance and partitioning model to determine the effective lubricant temperature in transit through the contact, and thus its effective viscosity. The heat flow to the surfaces determines their flash temperature, which in turn adjusts the lubricant inlet temperature for the subsequent instance of contact. This overall analytical approach has not hitherto been reported in literature.

2- Theory

2.1- Hydrodynamic conjunction

Ma *et al* [6], Akalin and Newaz [7] and Mishra *et al* [8,9] have shown that the generated pressures in the partially conforming compression ring-bore contact are insufficient to cause any localised contact deformation. However, in parts of the engine cycle often the thickness of film is insufficient to guard against some direct surface interactions. Therefore, the film thickness may be described in terms of the gap between the two rough contiguous surfaces as (Patir and Cheng [11] and Akalin and Newaz [7]):

$$h_T(x,t) = h_0(t) + s(x) + \delta_1 + \delta_2 \quad (1)$$

where, h_T is the local gap as shown in Figure 1, h_0 is the minimum film thickness (clearance) and $s(x)$ is the profile of the ring along its face-width. δ_1 and δ_2 are the roughness amplitudes on the contiguous surfaces; the ring and the bore. Equation (1) assumes idealised peripheral conformance of the ring to the bore surface, thus a one dimensional transient analysis of the contact is sought. Haddad and Tian [20] show that this condition yields results which are representative of a more complex two dimensional contact analysis for thin rings, yielding large perimeter-to-ring thickness ratio (of the order of 30). The profile of the ring face-width, $s(x)$ is asymmetrical unlike the usually assumed parabola. It was measured and fitted with a polynomial of order 6 which is reported in Rahmani *et al* [21].

Reynolds equation for piston compression ring-bore contact with no side leakage of the lubricant becomes:

$$\frac{d}{dx}\left(\frac{h_T^3}{12\eta_e}\frac{dp}{dx}\right)=\frac{U_1+U_2}{2}\frac{\partial h_T}{\partial x}+\frac{\partial h_T}{\partial t} \tag{2}$$

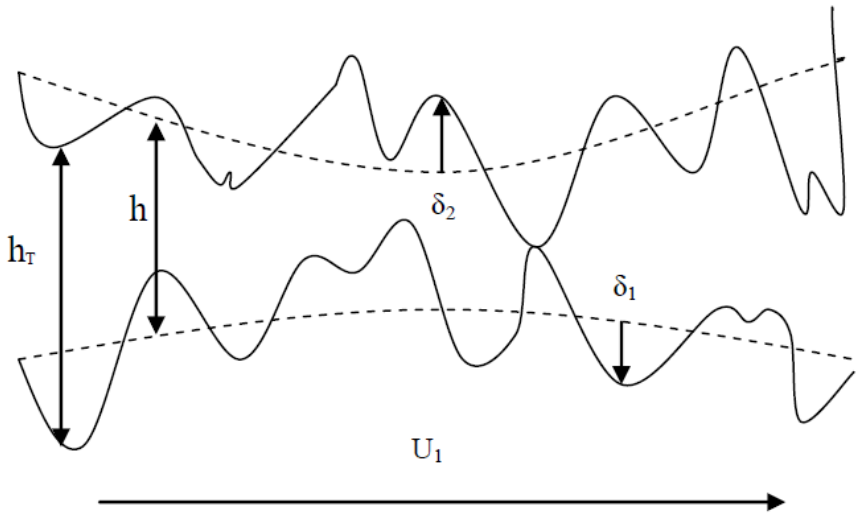

Figure 1: Film thickness shape in a rough contact

The roughness amplitudes are assumed to follow Gaussian distributions with mean of zero and standard deviations σ_1 and σ_2. Noting that the equivalent solid would be represented by the root mean square of the composite surface roughness, then: $\sigma=\sqrt{\sigma_1^2+\sigma_2^2}$. Replacing for h_T in equation (1), letting speed of entraining motion as: $U=(U_1+U_2)/2$ and contact factor $\varphi_c=dh_T/dh$, then [11]:

$$\frac{d}{dx}\left(\frac{\varphi_x h^3}{12}\frac{d\bar{p}}{dx}\right)=\eta_0\left(U\varphi_c\frac{dh}{dx}+\sigma\frac{\Delta U}{2}\frac{d\varphi_s}{dx}+\varphi_c\frac{dh}{dt}\right) \tag{3}$$

where, the sliding velocity is $\Delta U = |U_1 - U_2|$. Note that the piezo-viscous action of the lubricant due to relatively low hydrodynamic pressures is ignored as: $\alpha_0 p << 1$ [6,8].

Assuming no relative motions of the ring such as ring flutter or twist with respect to the piston, then the ring sliding speed is [22]:

$$\Delta U \approx r\omega\left(\sin\psi + \frac{r}{2\ell}\sin 2\psi\right) \tag{4}$$

Equation (3) is known as the average flow model, based on Reynolds equation. φ_x is the pressure-induced flow factor and φ_s the shear flow factor in the direction of entraining motion x (along the axis of the cylinder). These are functions of the Stribeck oil film ratio: $\lambda = h/\sigma$ (Appendix A). The average pressure is obtained as [7]:

$$\overline{p} = 6\Delta U\eta_e J_1 + 12\eta_e J_2\frac{\partial h}{\partial t} + C_1 J_3 + C_2 \tag{5}$$

where:

$$J_1 = \int_{-\frac{b}{2}}^{x}\frac{I_1 + \sigma\varphi_s}{\varphi_x h^3}dx, \quad J_2 = \int_{-\frac{b}{2}}^{x}\frac{I_2}{\varphi_x h^3}dx, \quad J_3 = \int_{-\frac{b}{2}}^{x}\frac{1}{\varphi_x h^3}dx \tag{6}$$

and

$$I_1 = \int_{-\frac{b}{2}}^{x}\varphi_c\frac{dh}{dx}dx, \quad I_2 = \int_{-\frac{b}{2}}^{x}\varphi_c dx \tag{7}$$

Heat is generated in the ring-bore conjunction by viscous shear of the lubricant as well as by the boundary friction produced by the contacting surface asperities.

The effective viscosity of the lubricant at the effective (average) lubricant temperature is found, using the Vogel [23] equation:

$$\ln\eta_e = \ln(0.158) + \frac{700.81}{\theta_e - 203} \tag{8}$$

The average temperature in the contact is then obtained as:

$$\theta_e = \theta_0 + \Delta\theta \tag{9}$$

Thus, the temperature rise $\Delta\theta$ must be obtained through thermal analysis in the contact.

2.2- Boundary conditions

The inlet boundary condition is set at the edge of the ring at pressure p_{in}. This position represents a drowned or fully flooded inlet. In practice, starvation of the contact may also occur. A fully flooded inlet is therefore assumed, extending to the edge of the ring face-width at $x = -b/2$. The coordinate system is set so that U remains always positive. Therefore, in the upstroke sense of the piston, p_{in} is the combustion chamber pressure and in the down-stroke, p_{in} is the crank-case pressure. Thus:

$$p = p_{in} \text{ at } x = -\frac{b}{2} \tag{10}$$

It is assumed that the ring rests on its lower and upper retaining groove lands in the up-stroke and down-stroke motions respectively [24].

Swift [25]-Stieber [26] exit boundary is assumed at the outlet from the conjunction, thus:

$$p = p_c, \ \frac{dp}{dx} = 0 \text{ at } x = x_c \tag{11}$$

where, p_c is the cavitation pressure at the oil film rupture position x_c found by equation (12). If the value of $x_c \geq b/2$, then no cavitation occurs and $p = p_{out}$ at $x = b/2$.

The Swift-Stieber boundary condition only predicts the film rupture point and does not address the lubricant film reformation which occurs beyond it as shown by the more complex JFO (Jakobsson and Floberg [27] and Olsson [28]) boundary conditions. Implementation of the JFO boundary is based on a set of boundary conditions for a partial film for Couette continuity alone which precludes an analytical solution as described here. Furthermore, a detailed study by Arcoumanis *et al* [29] has shown best fit results to the experimental findings are obtained with the Swift-Stieber exit boundary condition. Therefore, using the boundary conditions in equation (11), it can be seen that: $C_2 = p_{in}$, and using the outlet boundary conditions two expressions are obtained for C_1 whose equality yields:

$$\frac{\left(p_c - p_{in}\right) - 6\eta_e \Delta U J_{1c} - 12\eta_e J_{2c} \dfrac{\partial h}{\partial t}}{J_{3c}} = -6\eta_e \left[\Delta U \left(I_{1c} + \sigma \phi_{sc} \right) + 2 \frac{\partial h}{\partial x} I_{2c} \right] \tag{12}$$

where the integrals I and J have as their upper limits: $x = x_c$. Therefore, the solution to (12) yields the value of x_c.

It should be noted that lubricant film reformation clearly occurs continually as measured by Lee *et al* [30], otherwise the flow through the ring-pack would cease, which is clearly not the

case. The film reformation leads to lubricant flow reforming and the pressure reaching the prevailing outlet pressure, such as the inter-rings' pressure. Therefore, the limitations of Swift-Stieber outlet conditions are acknowledged.

2.3- Friction under mixed hydrodynamic regime of lubrication

The average hydrodynamic shear stress is [31]:

$$\bar{\tau} = \pm\varphi_{fp}\frac{h}{2}\left(\frac{d\bar{p}}{dx}\right) - \frac{\eta_e \Delta U}{h}\left(\varphi_f \pm \varphi_{fs}\right) \tag{13}$$

in which the plus sign is used for the ring and the negative sign for the liner.

However, there are also resistive forces originating from the local pressures acting on the sides of the asperity-pairs in oblique contact. The associated stress distribution can be represented as follows [31]:

$$\tau_i = V_i\left(\varphi_{fp}h - h_T\right)\frac{d\bar{p}}{dx} - \frac{2\eta_e \Delta U}{h}V_i\varphi_{fs} \ , \ i \in 1,2 \tag{14}$$

where, the variance ratio is: $V_i = \sigma_i^2 / \sigma^2$.

Therefore, the total shear/resistive force acting on the rough surfaces becomes:

$$f_{vi} = l\int_{-b/2}^{x_c}\left(\bar{\tau} + \tau_i\right)dx \tag{15}$$

where, $l = 2\pi r_0$. Usually in calculating the total horizontal force acting on either of the contacting surfaces, the terms associated with the pressure gradient are neglected as the corresponding terms are much smaller than the terms associated with the sliding velocity. However, in the current analyses these terms are also included in calculating the friction force for the sake of completeness.

The regime of lubrication is mixed in the ring-bore conjunction at least in some parts of the engine cycle, such as at the piston reversals at the top and bottom dead centres. Therefore, the generated pressures in the conjunction are partly due to hydrodynamic film and partly because of contact of opposing asperities as:

$$p_a(x) = \frac{8\sqrt{2}}{15}\pi\left(\zeta\kappa\sigma\right)^2\sqrt{\frac{\sigma}{\kappa}}E^{'}F_{5/2}(\lambda) \tag{16}$$

where $\zeta\kappa\sigma$ is the roughness parameter, $E^{'}$ is the equivalent plane strain elastic modulus of the counterfaces and the Gaussian statistical function is of the form [19] with $j = 5/2$:

$$F_j(\lambda) = \frac{1}{2\pi}\int_{\lambda}^{\infty}(s-\lambda)^j e^{-s^2/2} ds \tag{17}$$

Therefore, the total contact load is:

$$W = W_h + W_a = \int \bar{p} dA_h + \int p_a dA \tag{18}$$

where, W_a is the share of load carried by the asperities and W_h is the hydrodynamic reaction. The incremental proportion of the contact area occupied by a film of lubricant is $dA_h = dA - dA_a$ in which the total asperity tip area in contact between the two surfaces at any given apparent elemental contact area $dA = ldx$ is:

$$dA_a = \pi^2 (\zeta\kappa\sigma)^2 F_2(\lambda) dA \tag{19}$$

The function $F_2(\lambda)$ is found from equation (17), where $j = 2$.

Thus, the boundary friction is obtained as:

$$f_b = \tau_0 \int dA_a + \varsigma W_a \tag{20}$$

where, it is assumed that a thin adsorbed layer of lubricant resides at the asperity summits and acts in accord with non-Newtonian Eyring shear stress τ_0. The boundary shear strength of the surfaces contributes to friction, given by ς. For surfaces with a ferrous-based oxide layer: $\varsigma = 0.17$ [32].

Thus, the overall friction is obtained as:

$$f = f_{vi} + f_b \tag{21}$$

2.4- Thermal analysis

An analytical method based on a control volume approach is used to calculate an average temperature for the lubricant in the contact as well as the rise in surface temperatures of the bounding contact surfaces. Within the contact, the rate of heat generation through friction is obtained as:

$$\dot{Q} = f \Delta U \tag{22}$$

Some of this heat is conducted through the bounding contacting surfaces; the liner $\dot{Q}_1$ and the ring $\dot{Q}_2$. The remainder is carried away by the lubricant (convection), $\dot{Q}_{cv}$. Hence (see Figure 2):

$$\dot{Q} = \dot{Q}_1 + \dot{Q}_2 + \dot{Q}_{cv} \tag{23}$$

Any heat conducted through small asperity pair contact interface is neglected, because asperity area of contact is less than 1% of the contact area as noted by Greenwood and Tripp [19].

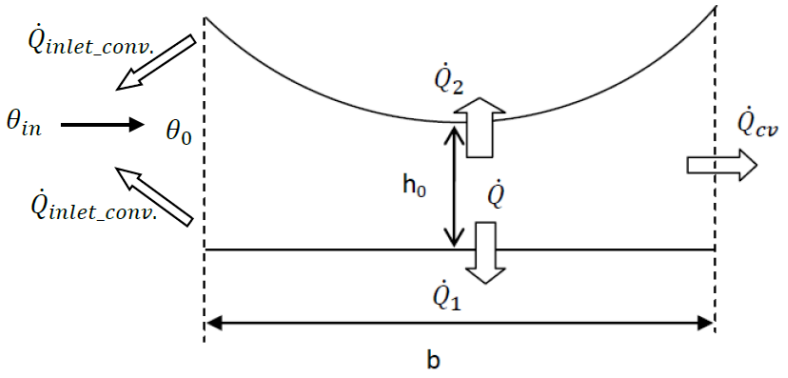

Figure 2: Thermal flow within the contact

The heat removal rate due to lubricant mass flow rate is:

$$\dot{Q}_{cv} = \dot{m} c_p \left(\theta_e - \theta_0\right) \tag{24}$$

where, the mass flow rate is obtained as [11]:

$$\dot{m} = \rho l \left\{ -\frac{\varphi_x h^3}{12\eta_e}\frac{d\overline{p}}{dx} + U h_T + \frac{\Delta U}{2}\sigma\varphi_s \right\} \tag{25}$$

At any instant of time, corresponding to a crank angle position, representing a small interval of time, equality of inlet and outlet flows is maintain. This is an outcome of the instantaneous quasi-static equilibrium at any given crank angle as indicated by equation (18). However, the flow rate is subject to change between subsequent crank angle positions.

There is a convection thermal flux at the inlet nib to the conjunction from the solid boundaries to the entrant lubricant supply at a lower temperature θ_{in}. This raises the inlet lubricant to θ_0 from its assumed bulk flow temperature as [33]:

$$\theta_0 = \frac{\theta_{s1}U_1 + \theta_{s2}U_2}{U_1 + U_2} \tag{26}$$

The initial temperature of the ring θ_{s2} is not known. Therefore, if one assumes the ring to be stationary and the liner to undergo relative motion, it is clear that: $\theta_0 = \theta_{s1}$ at the inlet due to the convective thermal flux. This is measured from the engine liner surface and input into the model at any given crank-angle location.

In the current analysis, the mass flow rate through the minimum gap has been considered as the representative flow through the compression ring-bore conjunction.

The lubricant density varies with temperature [34]:

$$\rho = \rho_0 \left[1 - \beta\left(\theta_e - \theta_0\right)\right] \tag{27}$$

where, β is the thermal expansion coefficient for the lubricant. It is usually considered to be around 6.4×10^{-4} K^{-1} [34, 35]. θ_0 is the inlet temperature of the lubricant, which is that of the liner/bore and θ_e is the effective (average) temperature of the lubricant in the contact, and c_p is the specific heat of the lubricant at constant pressure.

The heat carried away by the flow of lubricant is usually small compared with that conducted through the bounding surfaces. The dimensionless Peclet number is defined as [36]:

$$Pe = \left(\frac{Uh_0^2}{b}\right) / \left(\frac{k_l}{\rho c_p}\right) \tag{27}$$

The Peclet number is quite small in the case of ring-bore conjunction, particularly for the case of the engine considered in the current analysis. This is because the film thickness h_0 is quite thin. Hence, for all intent and purposes $\dot{Q}_{cv}$ can be ignored. However, for sake of generality convection heat flow is retained.

It is reasonable to assume that the heat is generated at the centre of the lubricant film. Olver and Spikes [33] assume the same and refer to some experimental evidence from traction tests. Then, the heat flowing to the bounding surfaces has to overcome a number of thermal resistive barriers (Figure 3). These are the resistances due to (i)- the lubricant film thickness; R_l, (ii)- the convective heat transfer through the boundary layer; R_v and (iii)- a rise in the solid surface flash temperature; R_f, where:

$$R_l = \frac{h_0}{2k_l A},\ R_v = \frac{1}{h_t A} \text{ and } R_f = \frac{S_f}{k_s A} \tag{28}$$

where, h_t is the heat transfer coefficient of the thin boundary layer and k_s is the thermal conductivity of the solid surface and $h_0/2$ is the characteristic length.

To obtain the convective heat transfer coefficient, h_t, the laminar flow of lubricant through the conjunction is considered to be analogous to fluid flow through a tube with fully developed velocity and temperature profiles, where L_{ev} and L_{eth} are defined as entrance lengths required for fully developed velocity and temperature profiles to take hold [37]:

$L_{ev} = 0.0565 h_0 \,\mathrm{Re}$ where, the Reynolds number, $\mathrm{Re} = \dfrac{\rho U h_0}{\eta_e}$ (29)

and $L_{eth} = 0.053 h_0 \mathrm{RePr}$ where, the Prandtl number, $\mathrm{Pr} = \dfrac{\eta_e c_p}{k_l}$ (30)

Since the condition (31) below holds in the case of current analyses:

$$\frac{L_{ev}}{b} << 1 \text{ and } \frac{L_{eth}}{b} << 1 \tag{31}$$

then, the Nusselt number becomes [37]:

$$Nu = \frac{h_t h_0}{k_l} = 4.36 \tag{32}$$

from which the heat transfer coefficient can be determined.

The thermal resistive barriers in equation (28) are represented as the required thermal power slopes per K , thus have the units WK^{-1} . Hence S_f is a characteristic length. The temperature of the bore surface is assumed to rise as the contact progresses. The characteristic length S_{f1} is therefore a function of thermal diffusivity of the surface $k_{s1}/\rho_{s1}c_{s1}$ and the average contact transit time $2b/\Delta U$. Hence using the solution given by Sharif *et al* [38]:

$$S_{f1} = \sqrt{\frac{2k_{s1}b}{\rho_{s1}c_{s1}\Delta U}} \tag{33}$$

The ring surface is always in contact with the heat source throughout its motion. Therefore, viewed as unwrapped, it can be assumed that the ring rectangular surface area is supplied with a steady heat flow at any crank angle. As a result, the characteristic length for the ring, S_{f2} would be [39]:

$$S_{f2} = \frac{1}{\pi A}\left\{ bl^2 \sinh^{-1}\left(\frac{b}{l}\right) + lb^2 \sinh^{-1}\left(\frac{l}{b}\right) + \frac{1}{3}\left[l^3 + b^3 - \left(b^2 + l^2\right)^{3/2} \right] \right\} \tag{34}$$

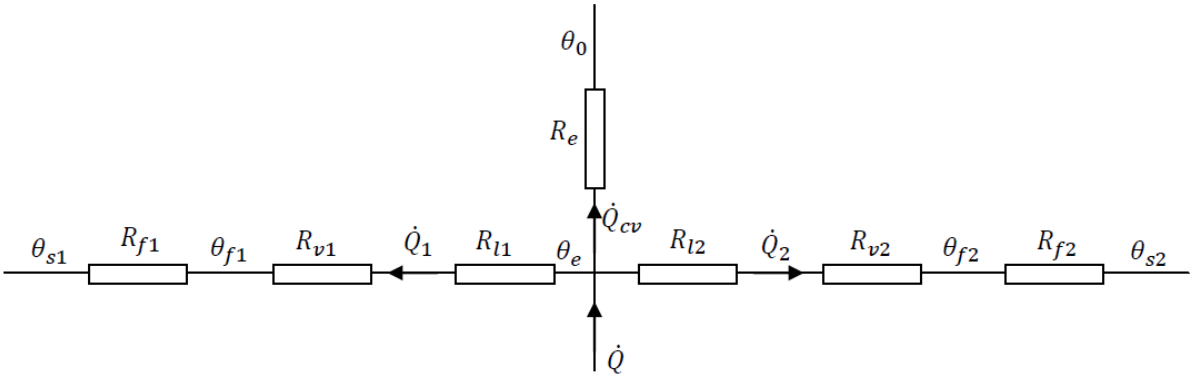

Figure 3: Heat transfer within the contact

Therefore, the heat conducted through to each surface (Figure 2) becomes:

$$\dot{Q}_i = \frac{\Delta\theta_i}{R_i} = \frac{\Delta\theta_i}{R_{li} + R_{vi} + R_{fi}},\ \Delta\theta_i = \theta_e - \theta_{si},\ i \in 1,2 \tag{35}$$

where, $i = 1$ is for the liner/bore surface and $i = 2$ is for the ring surface and θ_{si} are the initial temperatures of the surfaces.

Now replacing for in the heat balance equation (23):

$$\dot{Q} = \sum_{i=1}^{2} \frac{\left(\theta_e - \theta_{si}\right)}{R_i} + \frac{\theta_e - \theta_0}{R_e} \tag{36}$$

where, the thermal conductive flow barrier in lubricant flow; $R_e = 1/\dot{m}c_p$. Thus, the average (effective) lubricant temperature is obtained as:

$$\theta_e = \frac{\left(\dot{Q}R_e + \theta_0\right)\prod_{i=1}^{2} R_i + R_e \sum R_i \theta_{sj}}{\prod_{i=1}^{2} R_i + R_e \sum_{i=1}^{2} R_i},\ i, j \in 1,2 \text{ and } i \neq j \tag{37}$$

This effective temperature is used to determine the effective viscosity of the lubricant; equations (8) and (9).

Once, the effective lubricant temperature θ_e is obtained from equation (37), the temperature of the bounding solids is found through heat partitioning method (figure 3). To predict the surface temperatures, it is necessary to obtain the heat transferred to them; $\dot{Q}_i,\ i \in 1,2$. This is a relatively simple method with the current analytical approach. The proportion of generated heat transferred to the liner surface is denoted by χ_1, whilst that conveyed to the moving ring

surface is χ_2 and that convected by the lubricant flow through the contact is: $\chi_3 = 1-(\chi_1+\chi_2)$. Hence:

$$\chi_i = \frac{\dot{Q}_i}{\dot{Q}} = \frac{\Delta\theta_i}{\dot{Q}R_i},\ i \in 1,2 \tag{38}$$

and:

$$\chi_3 = 1-\sum_{i=1}^{2}\chi_i = \frac{\dot{Q}_{cv}}{\dot{Q}} = \frac{\theta_e-\theta_o}{\dot{Q}R_e} \tag{39}$$

Hence, using (38) and (39), the rises on surface temperatures are obtained as:

$$\Delta\theta_i = \left(\frac{S_{fi}}{k_{si}A}\right)\chi_i\dot{Q} = \frac{R_{fi}}{R_i}(\theta_e-\theta_{si}) \tag{40}$$

3- Method of Solution

The following procedure is used:

Step 1: At any crank-angle an outward force, adhering the ring to the bore surface, is calculated as:

$$F = F_e + F_g \tag{41}$$

where, the gas force is assumed to act behind the inner rim of the ring:

$$F_g = p_g bl \tag{42}$$

The ring tension force:

$$F_e = p_e bl \tag{43}$$

where, the elastic pressure [40]:

$$p_e = \frac{gEI}{3\pi b r_0^4} \tag{44}$$

where g is the end gap of the incomplete circular ring prior to fitment, and for a ring of rectangular cross-section: $I = \frac{1}{12} b d^3$.

Step 2: With an initial guess of $\eta_e = \eta_0$ for viscosity and h_0 for minimum film thickness the pressure distribution is obtained from equation (5) using the boundary conditions in (10) and (11) and by determining the film rupture point from (12) with contact kinematics given by equation (4).

Step 3: The Stribeck oil film parameter, $\lambda(x)$ is obtained and thus $p_a(x)$. This leads to the solution of equation (18) and the contact reaction *W*.

Step 4: The contact reaction is assumed to equilibrate the applied load from step 1; equation (41). Thus, the following convergence criterion is applied at any crank-angle, ψ:

$$\left| \frac{W - F}{F} \right| \leq \varepsilon \tag{45}$$

where, in the current study $\varepsilon = 10^{-4}$. If the convergence criterion is satisfied the crank angle is advanced, otherwise the nominal clearance h_0 is adjusted and the steps 2 through 4 are repeated:

$$h_0^n = \left(1 + B\vartheta\right) h_0^{n-1} \tag{46}$$

where, *B* is a damping coefficient, with the value of 0.005 in the current analysis. *n* is an iteration counter, and $\vartheta = \frac{W - F}{\max\{W, F\}}$.

Step 5: Friction is calculated using equations (15), (20) and (21). The power loss is now obtained using: $P = f \Delta U$. For an isothermal solution the analysis advances to step 1 for the next crank angle.

Step 6: The generated heat is obtained using equation (22). Heat convected by flow of lubricant is obtained using equations (24) and (25). Conducted heat through the bounding solids is obtained from equation (35).

Step 7: The effective (average) temperature of the lubricant in the contact is calculated, using equation (37) and the effective lubricant viscosity and density are obtained from equations (8) and (26) respectively. The steps 1 through 4 are repeated. When the convergence criterion is satisfied, the crank angle ψ is advanced by one degree and the entire procedure is repeated until all the 4-strokes in the engine cycle are completed and reached to a periodic state.

4- Results and Discussion

The analysis carried out here corresponds to a typical cylinder of a V12 engine with an output power of 510 BHP. Tables 1-4 provide all the necessary data for the current analyses.

Table 1: Engine data

Parameter	Value	Unit
Crank-pin radius, r	39.75	mm
Connecting rod length, ℓ	138.1	mm
Bore nominal radius, r_0	44.52	mm
Ring face-width, b	1.15	mm
Ring thickness, d	3.5	mm
Ring free end gap, g	10.5	mm

Table 2: Ring and liner mechanical/thermal properties

Parameter	Value	Unit
Liner material	Grey cast iron	-
Young's modulus of elasticity for liner material	92.30	GPa
Liner Poisson's ratio	0.211	-
Density for liner material	7200	Kgm^{-3}
Thermal conductivity for liner material	55	$Wm^{-1}K^{-1}$
Specific heat capacity for liner material	460	$Jkg^{-1}K^{-1}$
Ring material	Steel SAE 9254	-
Young's modulus of elasticity for ring material	203	GPa
Ring's Poisson's ratio	0.3	-
Ring coating material	Chromium Nitride (CrN)	-
Young's modulus of elasticity for CrN	400	GPa
Poisson's ratio for CrN	0.2	-
Thermal conductivity of CrN	12.134	$Wm^{-1}K^{-1}$

Table 3: Lubricant properties

Parameter	Value	Unit
Lubricant density	849.7 @ 15 [°C], 833.8 @ 40 [°C]	Kgm^{-3}
Kinematic viscosity	59.99 @ 40 [°C], 9.590 @ 100 [°C]	$\times 10^{-6}\ m^2s^{-1}$
Thermal conductivity	0.225 @ 120 [°C]	$Wm^{-1}K^{-1}$
Specific heat capacity	2360 @ 120 [°C]	$Jkg^{-1}K^{-1}$
Thermal expansion coefficient	6.5×10^{-4}	K^{-1}

Table 4: Ring and liner surface topography

Parameter	Value	Unit
Ra for liner	0.26	μm
Ra for ring	0.235	μm
Roughness parameter ($\zeta\kappa\sigma$)	0.04	-
Measure of asperity gradient (σ/κ)	0.001	-

Figure 4 shows (a)- the combustion pressure variation and (b)- piston sliding speed for engine speeds of 2000 and 6000 rpm respectively, as well as (c)- the measured liner wall temperature from the top dead centre, repeated for all the engine strokes. This is considered as the inlet temperature to the conjunction, the assumption being that any free surface oil prior to the contact inlet is at the same temperature as that of the liner surface. These and Tables 1-4 constitute the input to the analyses carried out in this paper.

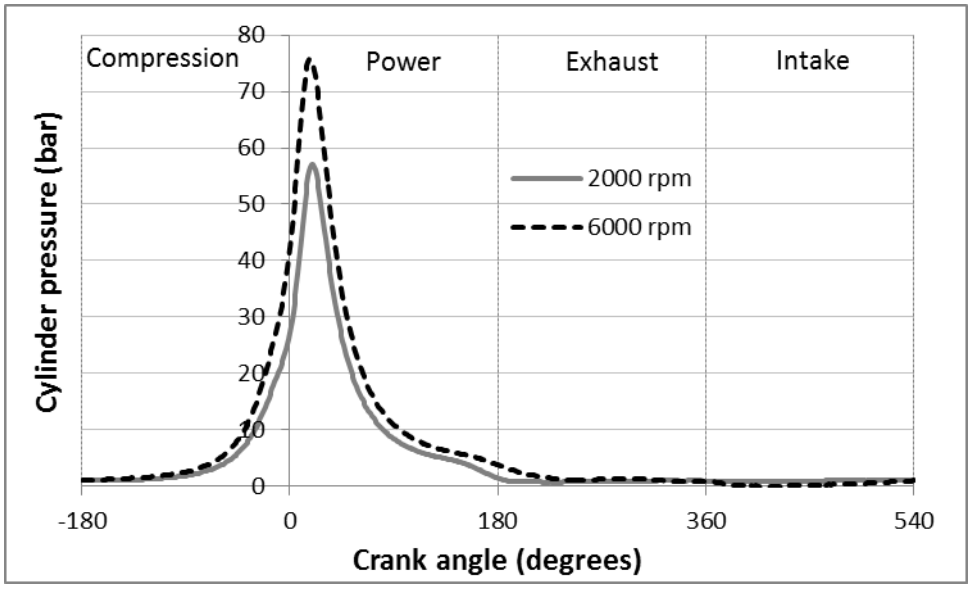
Compression
Power
Exhaust
Intake
2000 rpm
6000 rpm
Cylinder pressure (bar)
Crank angle (degrees)
80
70
60
50
40
30
20
10
0
-180
0
180
360
540

(a)

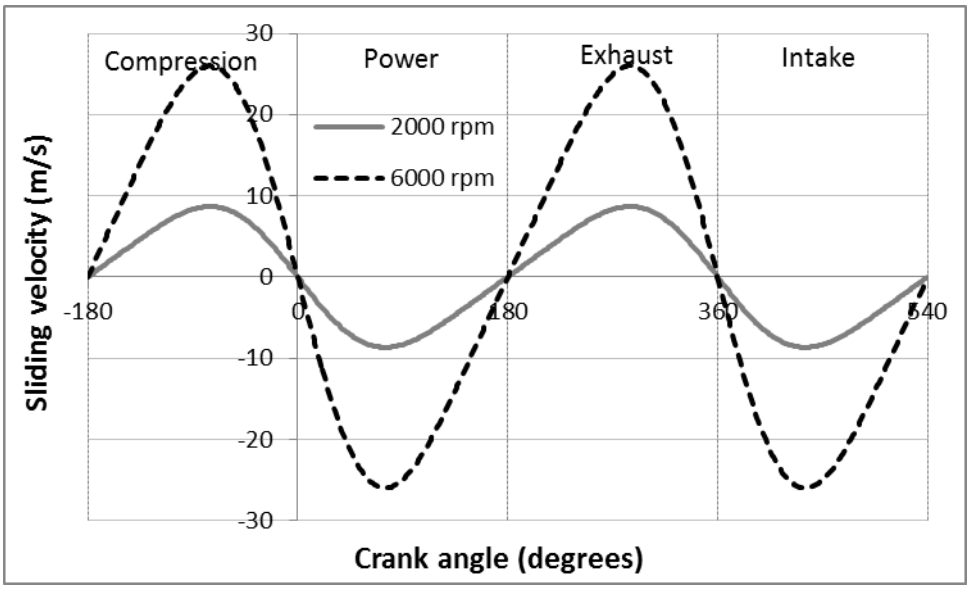
Compression
Power
Exhaust
Intake
2000 rpm
6000 rpm
Sliding velocity (m/s)
Crank angle (degrees)
30
20
10
0
-10
-20
-30
-180
0
180
360
540

(b)

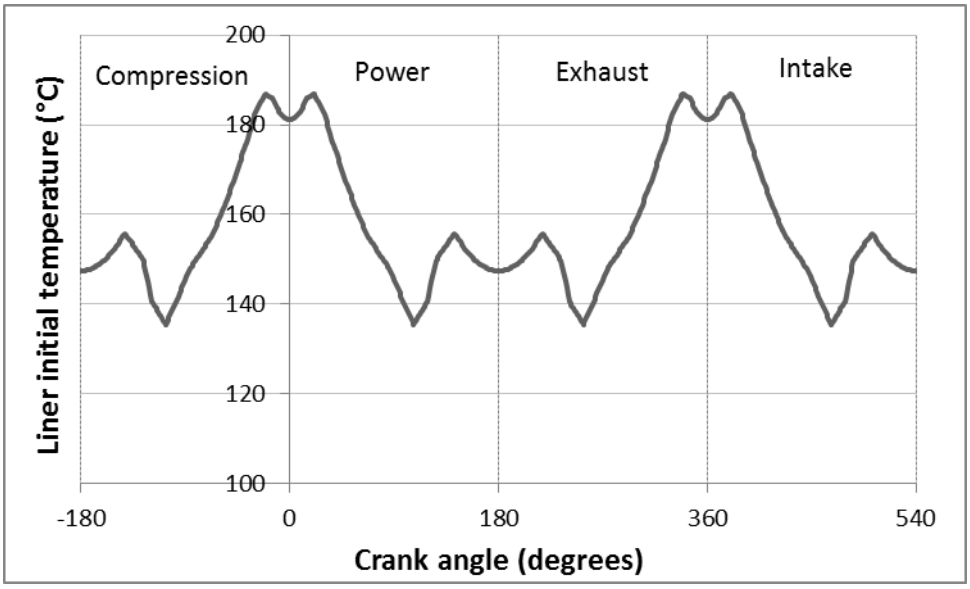

(c)

Figure 4: Input conditions to the analyses

Figure 5 shows the predicted minimum film thickness under isothermal (this corresponds to the analysis representing engine *cold* start conditions) and thermal conditions at the engine speed of 6000 rpm. The figure also includes the demarcation boundaries in accordance with Stribeck's proposition and based on the minimum clearance; $\lambda = h_0/\sigma$. These are at: $\lambda = 1$ (between boundary and mixed regimes of lubrication) and $\lambda = 4$ (between mixed and fluid film lubrication). Therefore, the predicted films in the interval $1 < \lambda < 4$ correspond to the mixed regime of lubrication. Thus, under isothermal condition, hydrodynamic regime of lubrication prevails for all the engine cycle except at the TDC reversal in progression from compression to the power stroke (crank angle of 0°) and every 720° thereafter. However, with thermal effects taken into account, the film thickness is considerably reduced and the ring-bore conjunction resides in mixed and boundary regimes of lubrication for a significant proportion of the engine cycle. Therefore, the assertion of significant differences between isothermal and thermal analyses by Gosh and Gupta [16] is justified, but not often noted in much of the reported studies.

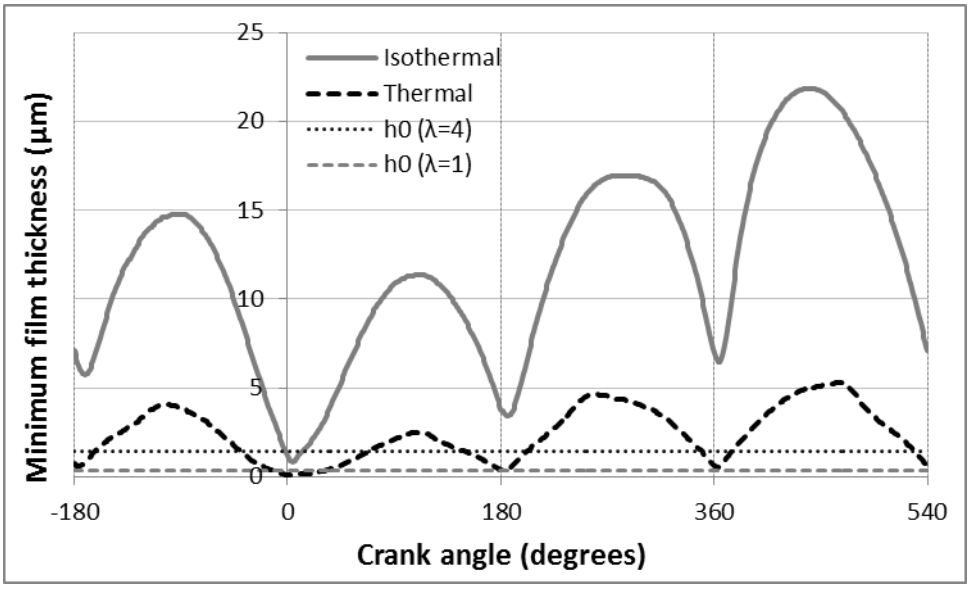

Figure 5: Predicted film thickness at the engine speed of 6000 rpm

It is instructive to note the effect of differences in Figure 5 upon friction and power-loss. Figure 6(a) shows the total friction (boundary and viscous contributions) for both isothermal and thermal analyses. Note that the isothermal analysis is representative of cold start-up condition, where the viscosity used in the analysis corresponds to lubricant temperature of 40^0C. The main contribution to friction under isothermal condition is through viscous shear of lubricant in all parts of the engine cycle except at the TDC in transition from compression to the power stroke ($\pm 5^\circ$ around TDC at the crank angle of 0°). The slope of friction rise rate does not follow the usual service parameter $\eta_0 \Delta U/h$ as is the case elsewhere. The slope is sharper on the account of asperity interactions. Elsewhere friction follows the sliding speed (a characteristic of viscous friction). In the case of thermal results, mixed regime of lubrication prevails in most of the engine cycle, thus friction rise or fall rate tends to follow the sliding speed with some deviation due to asperity interactions. In the vicinity of the TDC at 0° and BDC at 180° crank angle position (corresponding to transition from power to exhaust stroke) the regime of lubrication is momentarily boundary due to cessation of lubricant entraining motion. Friction, therefore, is manifested by a sharp spike there. The important point to note is that friction in general is lower in the thermal case and its main contribution is concentrated at dead centre reversals. This shows that for piston-bore system lubricant of lower viscosity is preferred. However, this *ideal* cannot be accommodated because the same engine oil flows through the higher load intensity contacts such as the cam-follower pair, where high loads necessitate use of lubricants which have sufficient load carrying capacity; i.e. high viscosity. This has been one of the main paradoxes in the development of engine oils for some time.

However, the concentration of main frictional contribution at the dead centres has provided the opportunity for surface modification such as laser texturing in the vicinity of reversal points. Readers can refer to [41-43] as representative examples.

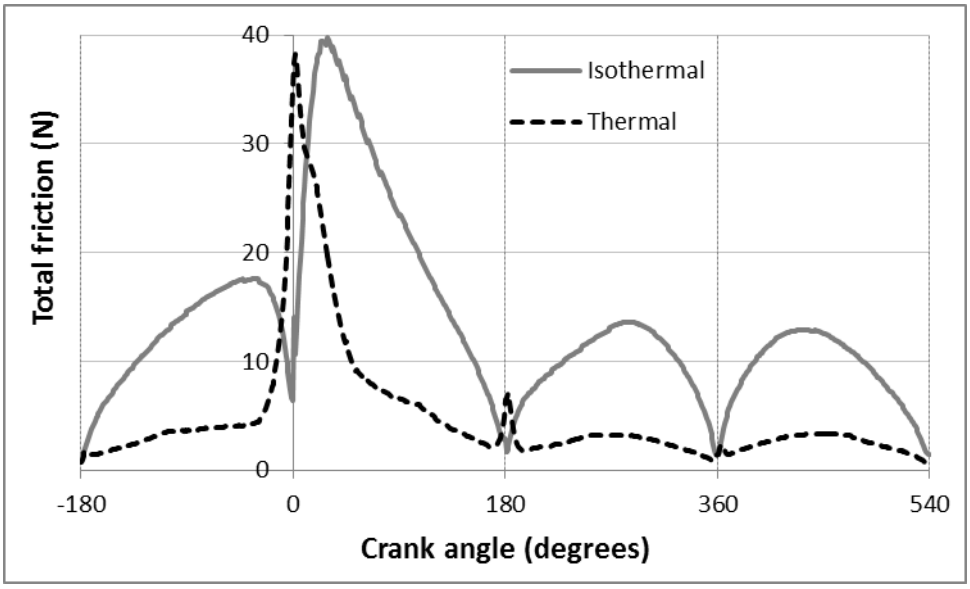

(a)

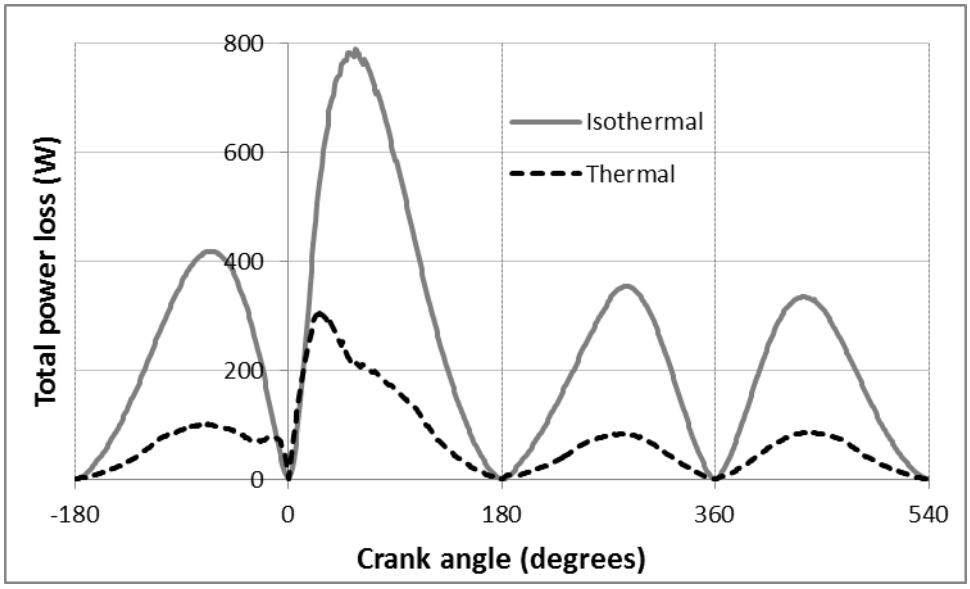

(b)

Figure 6: Friction and power loss through an engine cycle at 6000 rpm

The power loss in an engine cycle is shown in Figure 6(b). The same differences in characteristics can be noted as those observed from Figure 6(a) as the power loss is the function of friction and the sliding velocity. The key point to note is that power loss is considerably reduced after steady state condition is reached through thermal balance. In this sense the isothermal analysis may be envisaged as the worst conditions experienced before a thermal balance is reached, such as in cold start up. The two analyses are, therefore, the two ends of a spectrum of performance with transitory losses, commencing from a cold start up towards steady state thermal balance. This transition is clearly a function of driving cycle and

style. Changes in driving speed alters the sliding velocity and the combustion process, hence the power loss and thus the all-important fuel efficiency.

Figure 7 shows the contribution from boundary friction to the total friction under engine speeds for both the isothermal and thermal analyses cases. The results in Figures 7(a) and (b) show that in both cases, the contribution from boundary friction is significantly increased when thermal conditions are taken into account.

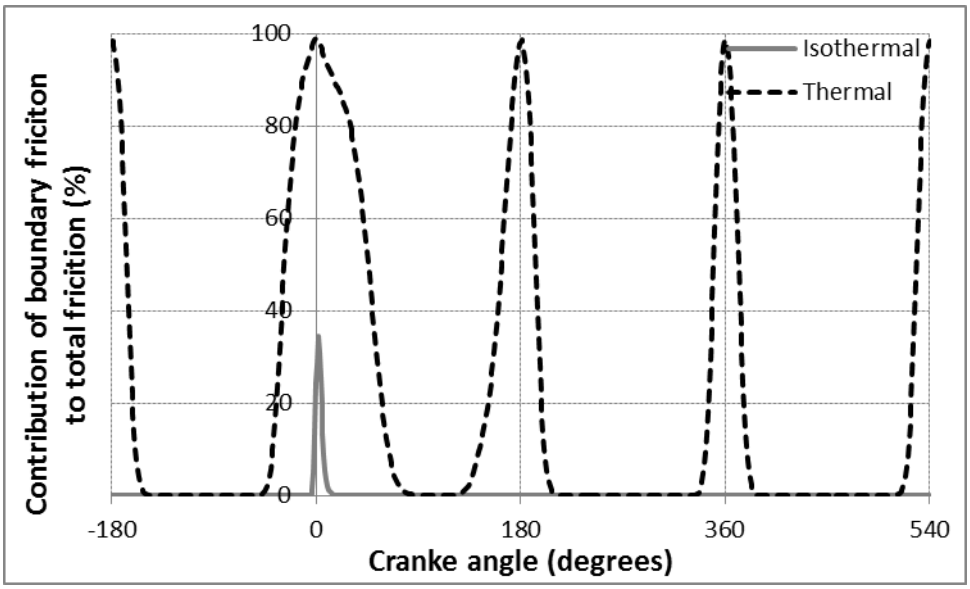

(a)

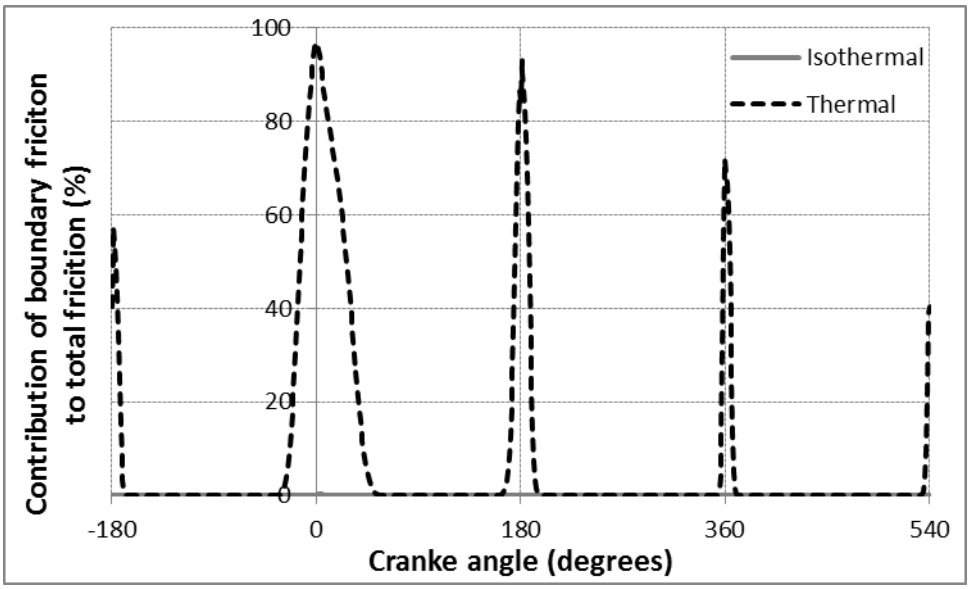

(b)

Figure 7: Percentage contribution to friction from boundary interaction through an engine cycle: (a)- at 2000 rpm and (b)- at 6000 rpm

At the higher speed of 6000 rpm, there is virtually no contribution from the asperity interactions when isothermal condition is assumed (Figure 7(b)). In general, it can be seen that at higher speeds the contribution from the asperity friction is reduced because a larger volume of lubricant is entrained into the contact with the assumed fully flooded inlet. Additionally, at the reversals there is greater contribution from squeeze film effect.

Changes in film thickness and the corresponding power loss for engine speeds of 2000 and 6000 rpm are shown in Figure 8. The higher speed corresponds to motorway driving under steady state condition, whilst the lower speed is representative of steady city driving. As expected the film thickness is reduced at the lower engine speed (Figure 8(a)).

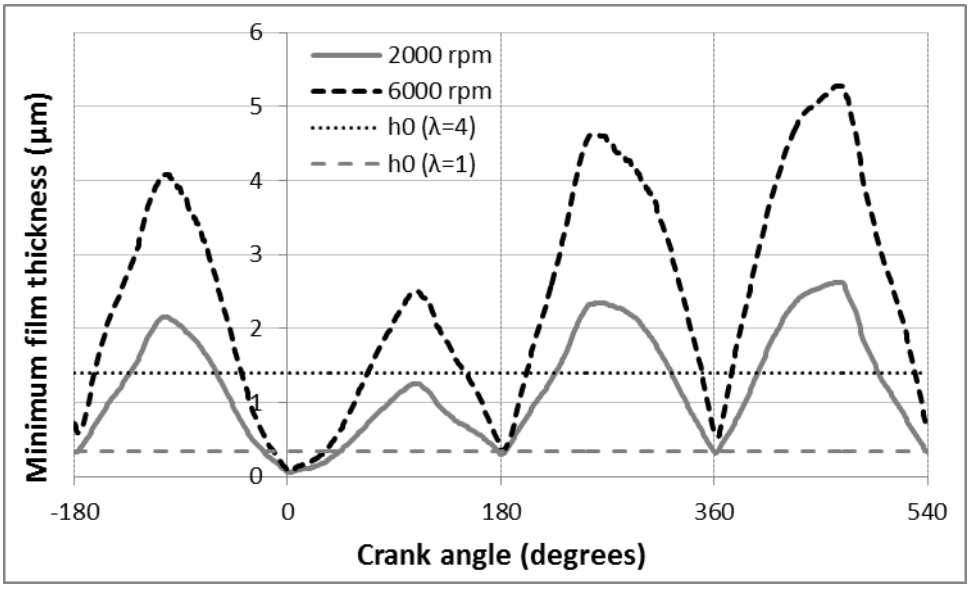

(a)

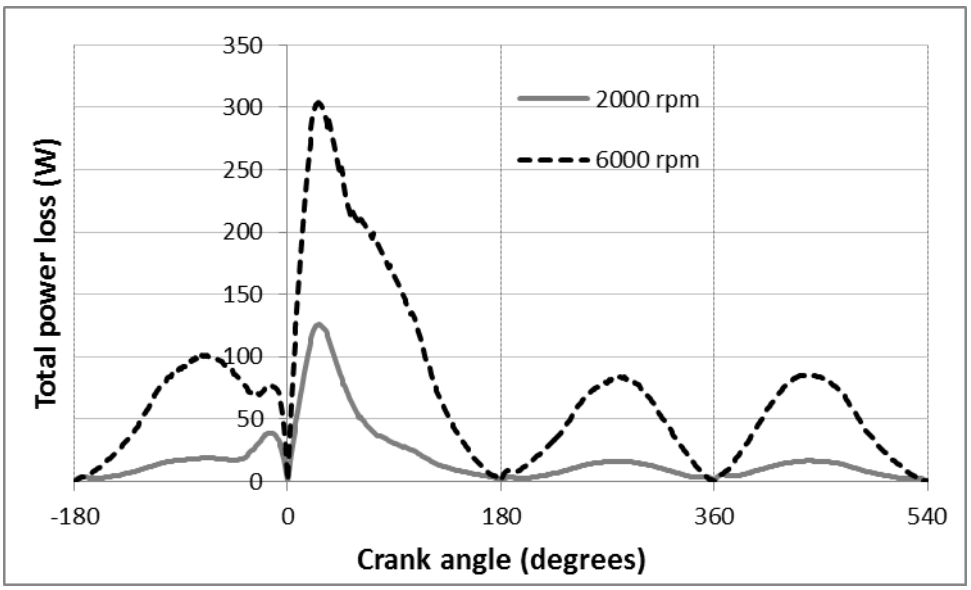

(b)

Figure 8: Lubricant film thickness and power loss under different driving conditions

The main contribution to cyclic power loss occurs at the TDC and the crank angle of 0° (Figure 8(b)). Elsewhere there is a rise in viscous friction at the higher speed, even with lower effective viscosity caused by a higher oil temperature rise (Figure 9). Therefore, the power loss is higher at the higher engine speed on the account of increased viscous friction at mid strokes and the increased sliding speed. An important point to note is that the transient temperature rise of the lubricant through the contact (short interval) is small compared with the surface temperature of the bounding solids when a thermal balance is reached. The temperature rise of a few degrees (Figure 9) is less than 5% of the surface temperature (Figure 4(c)). Hence, the effective viscosity of the lubricant is predetermined by the surface temperatures of the solids at the conjunction inlet. Therefore, for viscous friction the determining factor is the ratio $\Delta U/h$.

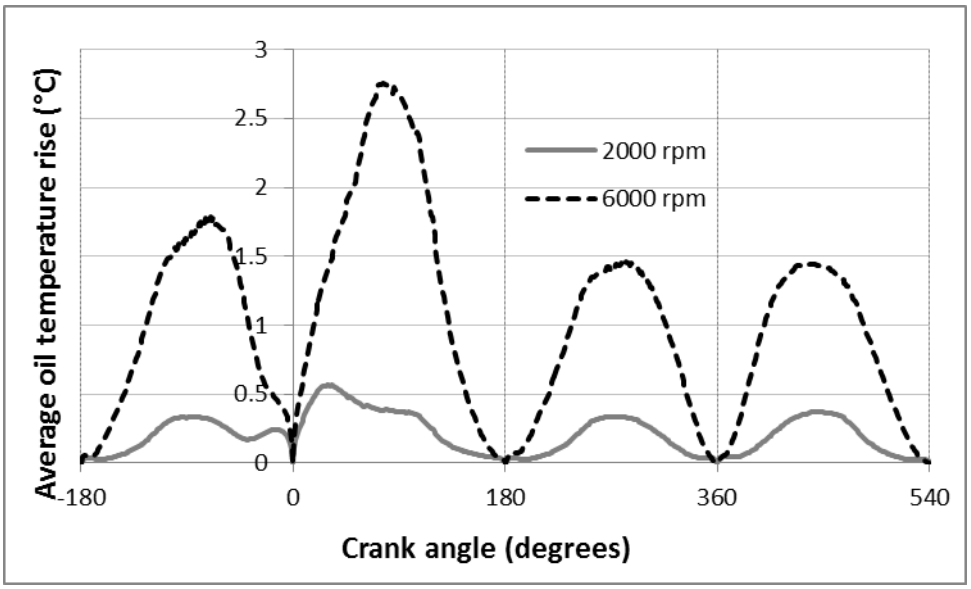

Figure 9: Lubricant temperature rise at different engine speeds

Therefore, instantaneous thermal balance plays an important role in the tribology of compression ring-liner/bore conjunction. This depends on a host of parameters which are more influential than the transitory heat generation within the contact itself due to friction. Firstly, the combination of engine cooling and heat generated by combustion determines the surface temperature of the liner/bore. As shown in Figure 1(b) the surface temperature of the liner far exceeds any rise in the contact temperature induced by friction (Figure 9). Thus, the temperature of the lubricant entering the contact is altered significantly from that of the bulk engine oil temperature at the nib of the contact through surface heat convection. Within the contact the temperature of the lubricant rises slightly above that of the faster moving surface (ring in this case, see Figure 10). The ring temperature remains higher than that of the liner because the film of lubricant clings to it and also on account of its poorer heat conductivity.

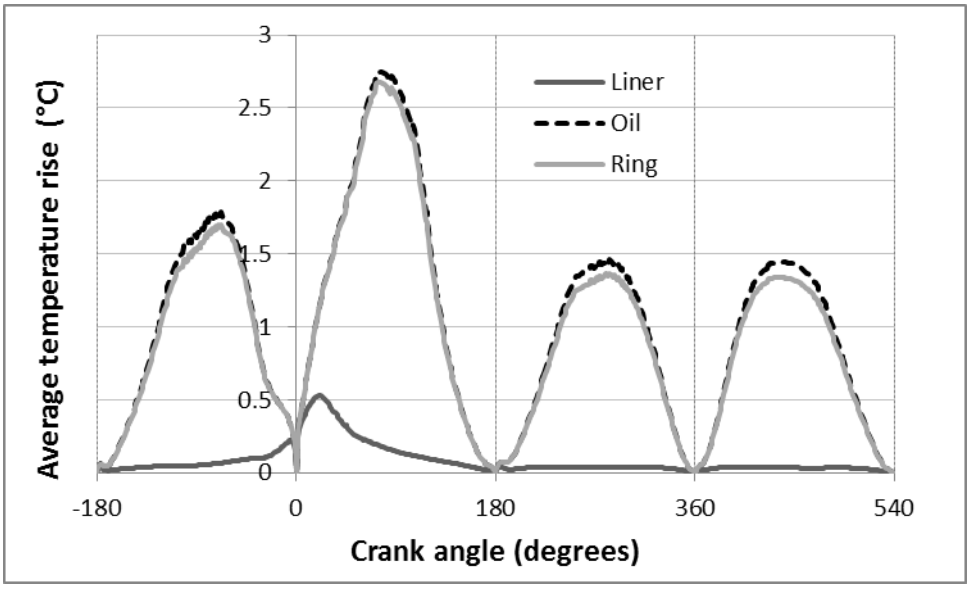

Figure 10: Temperature transience through contact transition in an engine cycle at 6000rpm

The liner temperature hardly rises as it conducts most of the heat away from the conjunction (Figure 11) and through to the coolant channels in the inter-bore space. Since, the heat generated in the contact is transitory; in line with the contact transition time, the steady state liner temperature is that governed by the balance of cooling and the temperature of combustion gasses. Therefore, the regime of lubrication is effectively determined by the engine block heat balance and the surface materials of the bounding solids and their topography as well as engine speed rather than the lubricant viscosity. The same is not true when the engine is cold, where lubricant rheology is the determining factor. These findings have been known or surmised experientially, but not confirmed through fundamental analyses. This represents the major contribution of the current fundamental study.

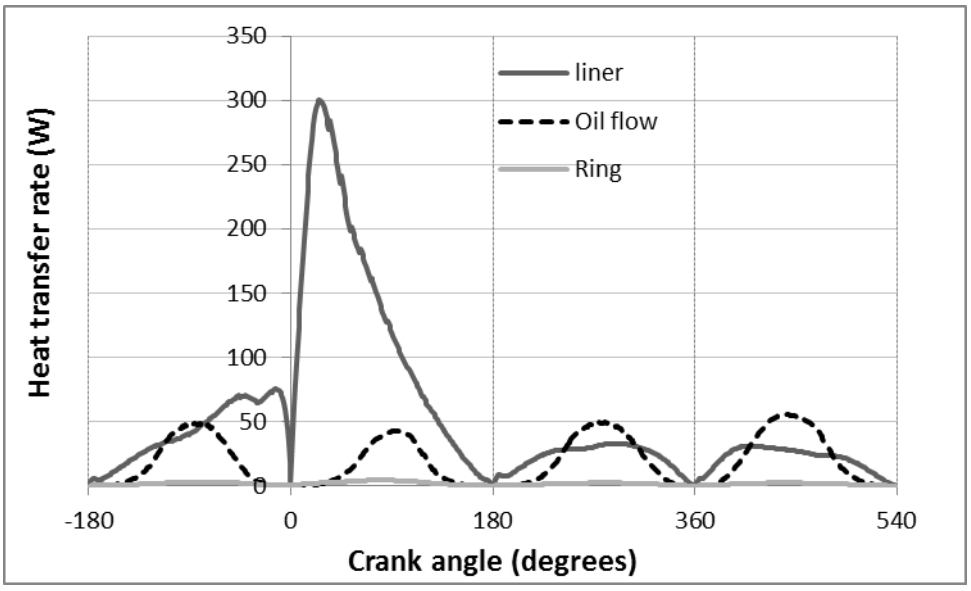

Figure 11: Contributions to heat transfer from the contact

5- Conclusions

The current analysis shows that thermal effects should be included in the study of ring-bore contact. The running surface temperatures of the contiguous solids are mainly influenced by the thermal balance between combustion gasses and the temperature of the coolant running through the inter-bore channels. Thermal balance is required between the surfaces and the heat generated through contact friction. Therefore, a detailed heat flow model is required, such as the one outlined in the current analysis. Friction generated heat is as the result of combined viscous shear of the lubricant film and the interaction of the ubiquitous asperities on the counterfaces. Therefore, a realistic model should encompass boundary interactions.

The predictions confirm shear thinning of the lubricant film under thermal mixed hydrodynamic regime of lubrication, whilst showing reduced power loss even with a considerable thinning of the lubricant film compared with an isothermal analysis. This is because the power loss due to viscous friction under isothermal condition throughout the engine cycle is actually larger than the losses of a thinner film with quite similar effective viscosity due to the small rise in lubricant temperature in the short contact transition time. Hence, isothermal analyses may be regarded as the cold engine condition and useful to predict the worst case scenario.

There are certain shortcomings in the current analysis. One is the use of one dimensional assumption along the ring face-width. This assumes good conformance of a thin ring to the bore surface, implying a right circular cylindrical bore, which is *idealised*. In practice the bore is out of round and ring-bore conformance is partial, leading to a non-symmetric ring-bore circumferential pressure distribution. Thus, a two dimensional analysis would be required. Another simplifying assumption concerns no relative motion between the ring and the piston, when within its retaining groove. In practice the ring flutters in the axial direction as well undergoing inertial motion and modal deformation in the radial direction. The former affects friction and contact kinematics, whilst the latter prohibits the assumption of instantaneous assumed load balance, which is underlying to the current analysis. Extending the current work to remove these implied assumptions constitutes the future direction of the current research.

Acknowledgements

The authors would like to express their gratitude to the Engineering and Physical Sciences Research Council (EPSRC) for the sponsorship of this research under the Encyclopaedic Program Grant (www.Encyclopaedic.org). Thanks are also extended to the other partner organisations, particularly in this instance to Aston Martin Lagonda for both its financial and technical support.

References

[1] Andersson BS. Company's perspective in vehicle tribology. in Dowson D, Taylor CM, Godet M, editors. Proc. 18th Leeds-Lyon Sympos. Elsevier; 1991, pp. 503-506.

[2] Dunaevsky VV. Analysis of distortions of cylinders and conformability of piston rings, STLE Trib. Trans.1990; 3: 33-40.

[3] Tomanik, E., 'Piston ring conformability in a distorted bore', SAE Paper No. 960356, 1996

[4] Lang TE. Vibration of Thin Circular Rings. Part 1, Jet Propulsion Lab. Tech.1962; Report No. 32-261.

[5] Tian KT. Dynamic behaviour of piston rings and their practical impact part 2: oil transport, friction and wear of ring/liner interface and the effects of piston and ring dynamics, Proc. Instn. Mech. Engrs., Part J: . Engng. Trib.2002; 216: 229-247.

[6] Ma M-T, Sherrington I. and Smith EH. Analysis of lubrication and friction for a complete piston-ring pack with an improved oil availability model – Part 1: circumferentially uniform film, Proc. IMechE, Part J: J. Engng. Trib.1997; 211: 1-15.

[7] Akalin O. and Newaz GM. Piston ring-cylinder bore friction modeling in mixed lubrication regime, Part I – analytical results. Trans. ASME. Series F: J. Trib. 2001; 123: 211-218.

[8] Mishra PC, Balakrishnan S. and Rahnejat H. Tribology of compression ring-to-cylinder contact at reversal, Proc. IMechE, Part J: J. Engng. Trib.2008; 222: 815-826.

[9] Mishra PC, Rahnejat H. and King PD. Tribology of the ring-bore conjunction subject to a mixed regime of lubrication, Proc. IMechE, Part C: J. Mech. Engng. Sci.2009; 223: 987-998.

[10] Dowson D, Ruddy B.L. and Economou, P.L. The elastohydrodynamic lubrication of piston rings, Proc. Roy. Soc. London, Series A, Mathematical and Physical Sciences 1983; 386 (1791): 409-430.

[11] Patir N. and Cheng H.S. An average flow model for determining effects of three-dimensional roughness on partial hydrodynamic lubrication, Trans. ASME, Series F: J. Lubn. Tech.1978; 100: 12-17.

[12] D'Agostino V. and Senatore A. Fundamentals of lubrication and friction of piston ring contact, in Rahnejat, H. (ed.) Tribology and dynamics of engine and powertrain – Fundamentals, applications and future trends, Cambridge, UK: Woodhead Publishing Ltd; 2010, Chapter 10.

[13] Chong WW F., Teodorescu M. and Vaughan N. Cavitation induced starvation for piston-ring/liner tribological conjunction, Trib. Int., 2010; 44(4): 483-497.

[14] Bolander N.W, Steenwyk B.D, Sadeghi F and Gerber G.R. Lubrication regime transitions at the piston ring-cylinder liner interface, Proc. IMechE. Part J: J. Engng. Trib. 2005; 219: 19–31.

[15] Furuhama S. and Sasaki S. New device for the measurement of piston frictional forces in small engines, SAE Paper No. 831284, 1983.

[16] Ghosh M.K and Gupta K. Thermal effect in hydrodynamic lubrication of line contacts – piezoviscous effect neglected, Int. J. Mech. Sci. 1998; 40: 603-616.

[17] Almqvist T. and Larsson R. The Navier-Stokes approach for thermal EHL line contact solutions, Trib. Int. 2002; 35: 163-170.

[18] Spencer A, Almqvist A. and Larsson R. A semi-deterministic texture-roughness model of the piston ring–cylinder liner contact, Proc. IMechE, Part J: J. Engng. Trib. 2011; DOI 10.1177/1350650110396279.

[19] Greenwood J.A. and Tripp J.H. The contact of two nominally flat rough surfaces, Proc. IMechE. 1970-1971; 185: 625-634.

[20] Haddad S.D. and Tian K-T. Analytical study of offset piston and crankshaft designs and the effect of oil film on piston slap excitation in a diesel engine, Mech. Mach. Theory.1995; 30: 271–284.

[21] Rahmani, R., Theodossiades, S., Rahnejat, H. and Fitzsimons, B. Transient elastohydrodynamic lubrication of rough new or worn piston compression ring conjunction with an out-of-round cylinder bore, Proc. IMechE, Part J: J. Engng. Trib., 2012; 226: 284-305

[22] Rahnejat H. Multi-body dynamics: Vehicles, Machines and Mechanisms. Joint Publishers: SAE, Warrendale, PA, USA and PEP (IMechE), UK, 1998.

[23] Vogel H. Das temperaturabhfingigkeitsgesetz der Viskosity on Fltissigkeiten, Physik Z.1921; 22: 645.

[24] Perera MSM, Theodossiades S, Rahnejat H. Elasto-multi-body dynamics of internal combustion engines with tribological conjunctions, Proc. IMechE, Part K: J. Multi-body Dyn.2010; 224 : 261-277.

[25] Swift HW. The stability of lubricating films in journal bearings. J. Inst. Civ. Engrs., 1932; 233(1): 267.

[26] Stieber W. Dus Schwimmlager. Verein Deutscher Ingenieurre, Berlin, 1933

[27] Jakobsson, B. and Floberg, L. The finite journal bearing considering vaporisation, Trans. of Chalmers University of Technology, 1957

[28] Olsson, K. O., Cavitation in dynamically loaded bearings, Trans. of Chalmers University of Technology. 1965

[29] Arcomanis, C., Duszynski, M., Flora, H. and Ostovar, P. Mixed lubrication modelling of Newtonian and shear thinning liquids in a piston-ring configuration, SAE pap No., 972924, 1997

[30] Lee, P.M., Priest, M. and Stark, M. The study of residence time and flow rate of lubricating oil through the top ring zone of a gasoline engine, ASME 2009 Internal Combustion Engine Div. Spring Tech. Conf., Pap. No. ICES2009-76134, pp. 793-801, 2009

[31] Patir N, Cheng HS. Application of average flow model to lubrication between rough sliding surfaces, Trans. ASME, Series F: J. Lubn. Tech., 1979; 101: 220-230.

[32] Teodorescu M, Balakrishnan S, Rahnejat H. Integrated tribological analysis within a multi- physics approach to system dynamics, Trib. & Interface Sci. Series, Elsevier, 2005; 48:725-737.

[33] Olver, A.V. and Spikes, H.A., 1998, Prediction of traction in elastohydrodynamic lubrication, Proc. IMechE, Part J: J. Engng. Trib., 1998, 212:321-332

[34] Yang P, Cui J, Jin, ZM, Dowson D. Transient elastohydrodynamic analysis of elliptical contacts. Part 2: thermal and Newtonian lubricant solution. Proc. IMechE, Part J: J. Engng. Trib.2005; 219: 187-200.

[35] Khan H, Sinha P, Saxena A. A simple algorithm for thermo-elastohydrodynamic lubrication problems. Int. J. Res. & Revs. in Appl. Sci. 2009; 1: 265-279.

[36] Gohar R and Rahnejat H. Fundamentals of Tribology, Imperial College Press, London, 2008.

[37] Suryanarayana NV. Forced Convection – Internal Flows. In: Kreith F, editor. The CRC Handbook of Thermal Engineering, USA: CRC Press LLC; 2000, Section 3.2.2, p. 3-47 to 3-55.

[38] Sharif KJ, Evans HP, Snidle RW, Newall JP. Modeling of film thickness and traction in a variable ratio traction drive rig . Trans. ASME, J. Trib. 2004; 126: 92-104.

[39] Carslaw HS, Jaeger JC. Conduction of heat in solids. 2nd ed. Oxford, UK: Oxford Science Publications, 2005.

[40] Bin Chik A, Fessler H. Radial pressure exerted by piston rings. J. Strain Anal. 1966; 2: 165-171.

[41] Rahnejat H, Balakrishnan B, King PD, Howell-Smith S. In-cylinder friction reduction using a surface finish optimization technique. Proc. IMechE, Part D: J. Auto. Engng.2006; 220: 1309-1318.

[42] Etsion I, Sher E. Improving fuel efficiency with laser surface textured piston rings, Trib. Int.2009; 42: 542-547.

[43] Etsion I. Surface texturing for in-cylinder friction reduction. In: Rahnejat H, editors. Tribology and Dynamics of Engine and Powertrain: Fundamentals, applications and future trends, Cambridge, UK: Woodhead Publications; 2010, p. 458-469.

[44] Chengwei W, Linqing Z. An average Reynolds equation for partial film lubrication with a contact factor. Trans. ASME, J. Trib.1989; 111: 188-191.

Appendix A:

The flow factors used are described below:

The pressure flow factor φ_x is calculated using an empirical relationship, shown by Patir and Cheng [11] as:

$$\varphi_x = 1 - 0.9e^{-0.56\lambda},\ \lambda > 0.5 \text{ and } \gamma = 1 \tag{A.1}$$

where γ is the ratio of correlation lengths in the *x* and *y* directions of the contact solids as described in [11]. It distinguishes between the various patterns of surface roughness. If an isotropic roughness is assumed, as in the current case, then clearly: $\gamma = 1$.
The shear flow factor is calculated using another empirical relationship stated as [31]:

$$\varphi_s = \begin{cases} 1.899\lambda^{0.98}\left(V_1 - V_2\right)e^{\left(-0.92\lambda + 0.05\lambda^2\right)}, & \lambda \le 5,\ \gamma = 1 \\ 1.126\left(V_1 - V_2\right)e^{-0.25\lambda}, & \lambda > 5,\ \gamma = 1 \end{cases} \tag{A.2}$$

Where V_1 and V_2 are the variance ratios $V_i = \frac{\sigma_i^2}{\sigma^2},\ i \in 1,2$

The contact factor for a partially lubricated conjunction is given as [44]:

$$\varphi_c = \frac{1}{2}\left[1 + erf\left(\lambda\right)\right] \tag{A.3}$$

The shear stress factors; φ_{fp}, φ_{fs} and φ_f are given in [31] as:

$$\varphi_{fp} = 1 - 1.4e^{-0.66\lambda},\ \lambda > 0.75,\ \gamma = 1 \tag{A.4}$$

$$\varphi_{fs} = \begin{cases} 11.1\lambda^{2.31}\left(V_1 - V_2\right)e^{\left(2.38\lambda + 0.11\lambda^2\right)}, & 0.5 < \lambda < 7,\ \gamma = 1 \\ 0, & \lambda > 7 \end{cases} \tag{A.5}$$

and:

$$\varphi_f = \begin{cases} \dfrac{35}{32}\xi\left\{\left(1-\xi^2\right)^3 \ln\left[300\left(1+\xi\right)\right]+\dfrac{1}{60}N\right\} & ,\ \lambda \le 3 \\ \dfrac{35}{32}\xi\left\{\left(1-\xi^2\right)^3 \ln\left(\dfrac{\xi+1}{\xi-1}\right)+\dfrac{\xi}{15}\left[66+\xi^2\left(30\xi^2-80\right)\right]\right\} & ,\ \lambda > 3 \end{cases} \qquad \text{(A.6)}$$

where: $\xi = \lambda/3$ and:

$N = \xi\left\{\xi\left[132+\xi\left(M+345\right)\right]\right\}-55$ and $M = \xi\left\{\xi\left[\xi\left(60+147\xi\right)-405\right]-160\right\}$